2D Materials

LETTER

Electronic properties of germanane field-effect transistors

B N Madhushankar[1], A Kaverzin[1], T Giousis[2], G Potsi[1,2], D Gournis[2], P Rudolf[1], G R Blake[1], C H van der Wal[1] and B J van Wees[1]

[1] Zernike Institute for Advanced Materials, University of Groningen, Groningen, NL-9747AG, The Netherlands
[2] Department of Materials Science and Engineering, University of Ioannina, 45110 Ioannina, Greece

E-mail: m.bettadahalli.nandishaiah@rug.nl

Abstract

A new two dimensional (2D) material—germanane—has been synthesised recently with promising electrical and optical properties. In this paper we report the first realisation of germanane field-effect transistors fabricated from multilayer single crystal flakes. Our germanane devices show transport in both electron and hole doped regimes with on/off current ratio of up to $10^5(10^4)$ and carrier mobilities of $150 \, cm^2 \, (V \cdot s)^{-1} (70 \, cm^2 \, (V \cdot s)^{-1})$ at 77 K (room temperature). A significant enhancement of the device conductivity under illumination with 650 nm red laser is observed. Our results reveal ambipolar transport properties of germanane with great potential for (opto)electronics applications.

The exceptional transport properties of graphene have generated an immense impulse that has stimulated the scientific community to study other layered Van der Waals materials [1–3]. Graphene analogues such as germanene, silicene, and stanene, as a separate family with hexagonal crystal structures, deserve careful consideration as they promise high quality charge transport properties, similar to their carbon predecessor [4, 5]. The hydrogenated form of germanene, known as germanane, has recently been synthesised for the first time by Bianco *et al* [9]. The crystal structure of germanane consists of a hexagonal germanium lattice with hydrogen atoms (H) covalently bonded to every germanium atom (Ge) as shown in figure 1(a). Germanane is of particular interest, because in addition to high quality charge transport it is expected to have a band gap, similar to its graphene analogue graphane [6–8]. In [9] the band gap of the germanane was experimentally estimated from diffuse reflectance absorption spectroscopy to be around 1.59 eV, close to the calculated values reported in [6–8]. Until now the number of available publications on this material is still very limited, covering theoretical investigation of the band structure [6–8, 10, 12] and very preliminary electrical characterisation [11, 13, 14]. The electron mobility, limited by electron-phonon scattering, was calculated to be around 20 000 $cm^2 \, Vs^{-1}$ at room temperature [9], which is strongly appealing for germanane to form a good basis for future application devices.

To prepare the multilayer germanane flakes from powder we followed the protocol from Bianco *et al* [9], which involves the topochemical deintercalation of $CaGe_2$. The quality of our germanane powder has been confirmed by a set of characterisation techniques including x-ray diffraction, FTIR spectroscopy, Raman spectroscopy and DRA measurements (see supplementary information stacks.iop.org/TDM/4/021009/mmedia), which fully verify that the synthesised material is indeed germanane. The prepared powder was further processed to fabricate transistors. Germanane flakes were mechanically cleaved down to thicknesses ranging from 15 nm up to 90 nm and placed on top of a 300 nm Si/SiO_2 substrate. Ti/Au contacts (5 nm/ 100 nm) were made via standard PMMA-based e-beam lithography, as shown in the optical image of a typical device in figure 1(b). The thickness of the flake was determined by atomic force microscopy (AFM) as shown in figures 1(c) and (d) to be ∼60 nm. Further details of the fabrication protocol are given in the methods section.

As initial electrical characterisation we performed resistance measurements at room temperature in the linear regime (the measured voltage scales linearly with the applied current). We measured the voltage V in a 2-terminal configuration when a constant current of 2 nA was supplied, shown as the blue curve in figure 2(a). The signal was measured as a function of the applied gate voltage V_G, revealing a peak-like feature. The appearance of this maximum is associated with tuning of the Fermi
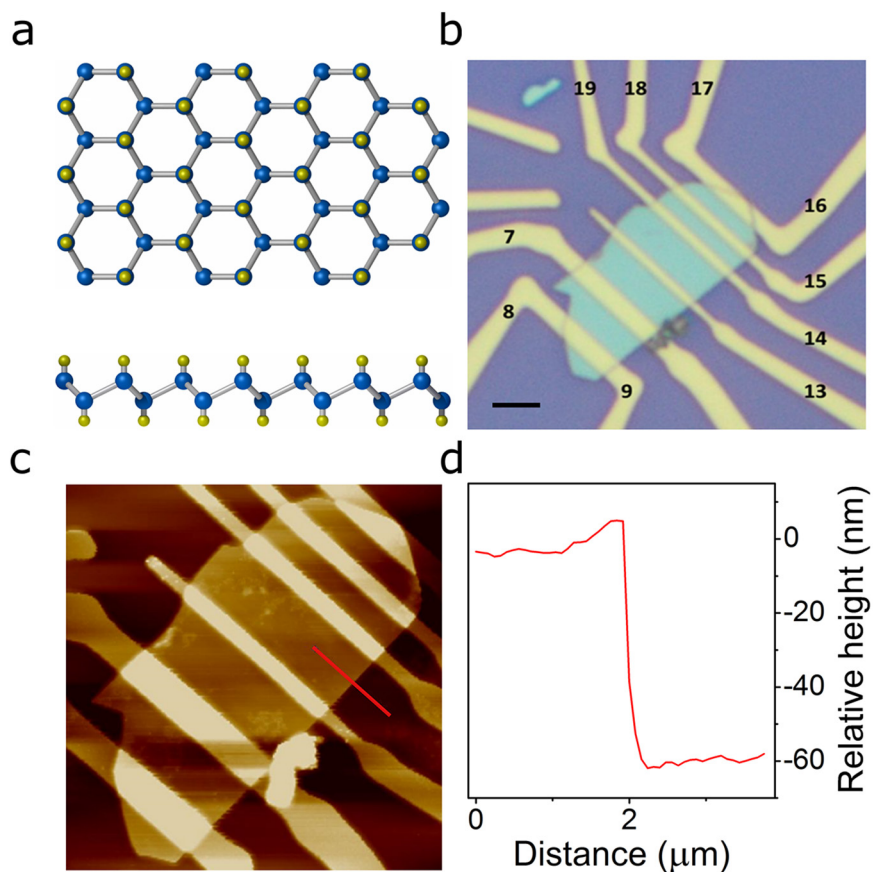
Figure 1. (a) Schematic representation of a germanane monolayer (top and side views) with Ge atoms (blue) at the corners of hexagons and H atoms (yellow) bonded to Ge. (b) Optical image of the germanane flake based device on top of a Si/SiO$_2$ substrate with Ti/Au electrodes (Scale bar is 3 μm). (c) AFM image of the germanane transistor. (d) The height profile is plotted along the red line as shown in panel (c) giving the flake thickness to be ∼60 nm.
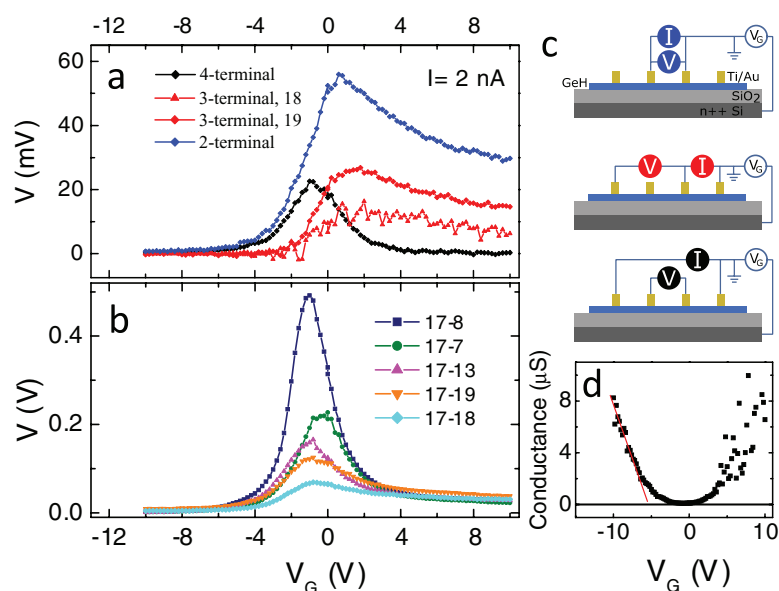
Figure 2. (a) Measured signal V plotted for 2-terminal (blue), 3-terminal (red) and 4-terminal (black) configurations as a function of the gate voltage. The 3-terminal measurements were performed using both contacts 18 (triangles) and 19 (diamonds). The applied constant current between source and drain was 2 nA, and the measurements were performed at room temperature. (b) 2-terminal measurements as a function of V_G performed using different distances between the contacts while keeping the same source contact. The resistance values at the curve maxima scale approximately with the channel length (for the sample geometry, see figure 1(b)). $I = 2$ nA. (c) 2-, 3- and 4-terminal measurement configurations allow the contact and channel-related resistances to be extracted separately. (d) Room temperature conductance calculated from the 4-terminal measurement shown in panel (a) The red line represents a linear fit resulting in a mobility of ∼30 cm^2 (V · s)$^{-1}$.

level of the material in the band gap, implying that the studied device is ambipolar or, in other words, indicating the possibility to electrically dope it with both holes and electrons. It is worth noting here that the position of the maximum close to $V_G = 0$ V indicates a relatively low intrinsic doping of the material.

A semiconductor, when brought into direct contact with a metal, forms a Schottky barrier which usually results in a relatively high contact resistance and thus affects the measured 2-terminal $V(V_G)$ dependence. To circumvent the influence of the resistive contacts and distinguish between channel and contact properties, 4-terminal electrode configuration was used. In figure 2(a) different multiterminal measurements (see figure 2(c) for schematics of configurations) are shown together for a clear comparison. The 2-terminal measurement contains contributions from both the channel resistance and the two interface resistances (see supplementary information for the resistance model used) and is seen to be asymmetric with respect to the peak position. In contrast, the 4-terminal voltage shows a much more symmetric dependence on V_G, as one would expect for a semiconducting material with similar electron and hole transport properties. The difference between the 2-terminal and 4-terminal curves is ascribed to the contact resistances and can be probed more directly in a 3-terminal configuration. The measured dependencies indeed indicate that the observed asymmetry is related to the transport through or in the vicinity of the contact interface and can be explained by the presence of the expected Schottky barriers at each contact interface. The degree and sign of the asymmetry (as for the height and position of the Schottky barrier itself) are determined both by the Fermi level positions in the adjacent regions and by the properties of the interface such as the density of impurity states. We note that in addition to formation of the Schottky barrier, the metal contact can also lead to modification of the underlying bulk channel. In this scenario the contact contribution cannot be excluded even in a 4-terminal configuration (see supplementary information for more details).

An alternative way to differentiate between the channel and contact properties is to measure 2-terminal resistances for different channel lengths. In figure 2(b) we plot 2-terminal resistances measured with fixed source contact 17 while the drain contact was varied over all possible configurations (see figure 1(b)). The central portion of the curves around the maxima scales approximately with the channel length L, while for large positive gate voltages the measured signals saturate at values that are independent of L. This further confirms a clear distinction between the channel associated resistance and the asymmetric contribution attributed to the contact regions, which influences the measurement mostly at positive V_G.

Next we replot the measured 4-terminal voltage in terms of the channel conductance (I/V) as a function of applied V_G, in figure 2(d). The obtained dependence is symmetric, emphasizing again the ambipolar-

ity of the transport. Assuming a linear dependence of the conductance on carrier concentration and that the geometrical capacitance per unit area of the bottom Si/SiO$_2$ gate is 11 nF cm^{-2}, we estimate a carrier mobility of $\sim$30 cm^2 (V $\cdot$ s)$^{-1}$ at room temperature.

In order to explore the higher carrier concentration regime, we extended the range of used gate voltages upto $\pm$50 V. At the maximum V_G range, an on/off current ratio for the holes is found to be $\sim$10^4 at room temperature and $\sim$10^5 at 77 K (see supplementary information available at stacks.iop.org/TDM/4/021009/mmedia). At $|V_G| > 10$ V a prominent hysteretic behaviour develops which is most pronounced at higher temperatures where the difference between the positions of the minima for opposite sweeping directions can be as large as $\sim$60 V for a sweeping range of $\pm$50 V (at a sweeping rate of $\sim$0.1 V s^{-1}). Such hysteresis indicates the presence of a substantial number of charge trap states within the range over which the Fermi level varies. Under an applied gate voltage these traps become activated/deactivated and can modulate the effective doping level of the system, thus affecting the shape of the conductivity dependence. At lower temperatures charge traps become frozen, considerably diminishing the degree of hysteresis and improving the reliability of the mobility estimation. For clarity, in our subsequent analysis below we use measurements performed with the same sweep direction from positive to negative V_G unless stated otherwise (figure 3). The mobility is estimated from the linear high carrier concentration part of the conductance dependence as a function of V_G and is plotted as a function of temperature in the inset. The observed increase in mobility with decreasing temperature could suggests a significant reduction of the contribution of the phonon scattering to the transport properties of carriers. Alternatively such temperature dependence of the extracted mobility can be artificially induced by the temperature dependent hysteretic behaviour of the measured conductance. However, such mobility extraction is still reliable at low temperatures where the observed hysteresis is minimal. Below about 170 K, the mobility saturates at $\sim$150 cm^2 (V $\cdot$ s)$^{-1}$. This exceeds the value estimated from the room temperature, low V_G range dependence (figure 2(d)), presumably due to the fact that in the low V_G range the system does not yet reach the linear conductivity regime as the Fermi level is still in the transition from the band gap to the valence band. Furthermore, electron transport is observed to be significantly suppressed compared to hole transport due to the presence of both hysteresis and the contact contribution in the 2-terminal measurement configuration as discussed earlier. Therefore, the set of performed measurements does not allow us to characterise the temperature dependence of the electron transport.

To further demonstrate the transistor action of germanane in the non-linear regime, we repeated the 4-terminal voltage measurements using applied currents up to 100 nA, as shown in figure 4. In this regime
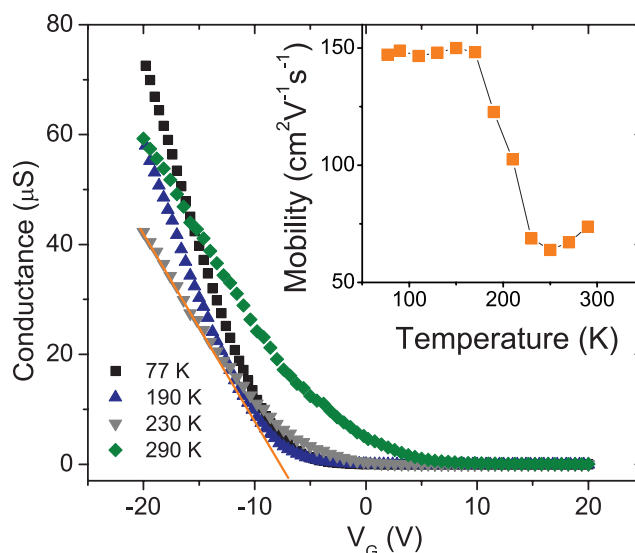
Figure 3. The 2-terminal conductance for contacts 18 and 19 is plotted as a function of V_G at different temperatures. The orange line represents an example of a linear fit for the extraction of hole mobility. The perceived 2-terminal hole mobility is expected to be close to the actual channel mobility because (as shown in figure 2) the contact contribution at negative gate voltages is minimal. The gate voltage was swept from positive to negative values. Inset: 2-terminal hole mobility extracted from the data plotted in the main panel, shown as a function of temperature.
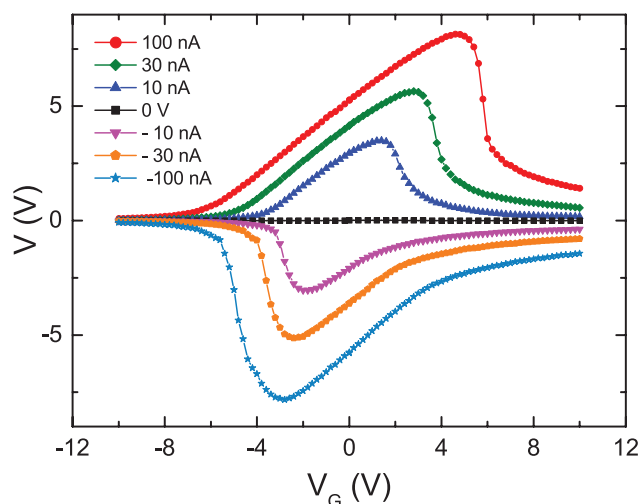
Figure 4. 4-terminal voltage measured as a function of V_G for a set of different bias currents at room temperature. The current was applied between contacts 17 and 7, while the voltage was measured between contacts 19 and 13.

the voltage drop along the channel becomes comparable with the applied gate voltage and therefore creates an easily observable additional doping effect that changes along the length of the transport channel. These transport measurements probe an effect that can be approximated to first order by an average doping value, i.e. an extra gating of $V/2$. This means that under an applied voltage V across the channel, the measured dependencies are expected to be shifted by $V/2$. Such a shift is indeed seen in figure 4. For instance, when the applied bias current is 100 nA the voltage across the sample at the maximum is $\sim$8 V. The position of the maximum is shifted with respect to its linear regime position (see figure 2(a)) by $\sim$5 V, which is close to the expected 8/2 V. The small degree of asymmetry between positive and negative applied currents indicates intrinsic asymmetry

in the device and is further discussed in the supplementary information.

So far we have presented measurements performed in the dark, thus avoiding influence of ambient light on the transport characteristics of germanane. However, the theoretical studies [6–8] suggest the presence of a direct band gap in germanane, which implies a substantial response of the material to light excitation of the appropriate wavelength. Accordingly, we performed an experiment where the channel conductance in 4-terminal configuration was measured both in the dark and under illumination, shown in figure 5. For the light source we used a red laser with a wavelength of 650 nm and an intensity of $\sim$40 mW cm^{-2}. The increase of the conductance under illumination over a certain gate voltage range (swept from negative
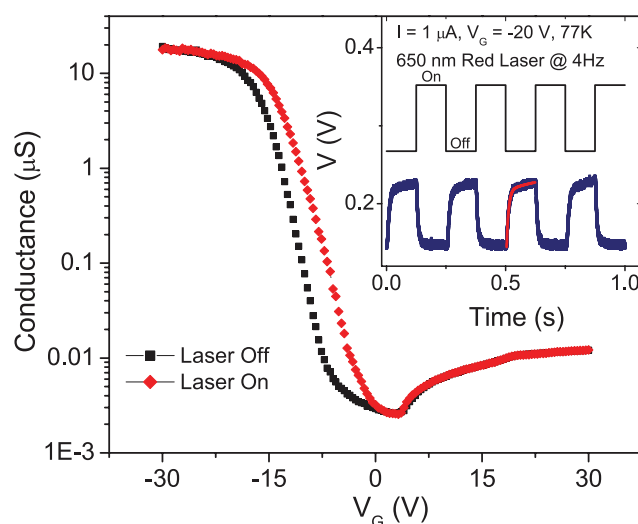
Figure 5. 4-terminal conductance shown as a function of the gate voltage measured in the dark (black squares) and under red laser illumination (red diamonds). The current was applied between contacts 17 and 8, while the voltage was measured between contacts 18 and 19. $I = 1\ \mu A$, $T = 77$ K. Inset: 4-terminal V plotted as a function of time when the laser is switched on and off with a chopper at 4 Hz. Applied $V_G = -20$ V, $I = 1\ \mu A$. The red curve represents a fit using a double exponential dependence resulting in two characteristic times, 8.3 ms and 0.20 s. The black line shows the laser intensity, plotted in arbitrary units, which was switched between 0 and ~ 40 mW cm^{-2}.

to positive values) can suggest the excitation of extra carriers by photons as it happens in direct band gap materials. However, the substantial hysteresis in the system that is also observed indicates the presence of charge traps in the channel or in its vicinity. Such trap states can also be optically active and can influence the response to the illumination. The time responses of a trap system and a band electron system are expected to be significantly different because band electron systems reach equilibrium relatively fast compared to trap states. In the inset to figure 5 we show the electrical response measured in 4-terminal configuration as a function of time when the laser light was modulated with a chopper at a frequency of 4 Hz. Double exponential fitting clearly indicates two components with characteristic times of $t_1 \approx 0.20$ s and $t_2 \approx 8.3$ ms. Since the trap-associated processes are expected to be much longer than those associated with band carriers, we interpret the appearance of a long time t_1 as an indication of trap states in the vicinity of the channel. The short time t_2 is consistent with the bandwidth limitation of our electrical measurement circuit (RC time limitation), which masks the real time scale of the fast response. The time response of band electrons in similar systems is typically faster than 1 ns (for GaAs see [15]). Therefore, further investigation with a higher frequency bandwidth is needed in order to characterise the photoresponse of the device at short timescales.

In conclusion, in this work we have demonstrated the realisation of single crystal germanane field-effect transistors with a current on/off ratio in the range of 10^4–10^5, depending on the temperature. By employing various multiterminal measurement configurations, we have clearly separated the transport properties of

the germanane channel from those of the contacts. Low gate voltage dependence measured at room temperature clearly reveals that germanane exhibits ambipolar behaviour. We have found a low bound for the hole mobility to be 70 cm^2 V·s^{-1} at room temperature which further increases to ~ 150 cm^2 V·s^{-1} below 150 K. Moreover, our study of the influence of light illumination confirms the high responsivity of the material, although further investigations are needed to fully characterise the photoresponse.

Methods

Germanane (GeH) was synthesised by the topotactic deintercalation of β-CaGe$_2$ in aqueous HCl at -40 °C based on a method reported previously [9, 16–18]. The precursor phase β-CaGe$_2$ was prepared by sealing a stoichiometric 1 : 2 ratio of calcium (granular Ca with purity 99 % from Sigma-Aldrich) and germanium (Ge powder with purity 99.99%, Sigma-Aldrich) in a cylindrical alumina crucible (external diameter of 11 mm) enclosed in an evacuated fused quartz tube (internal diameter of 12 mm). The mixing of the two metals and the filling of the crucible was performed in a glove box under nitrogen atmosphere. The sealed quartz tube was then placed in a box furnace and the following temperature profile was employed: (1) heating to 1025 °C within 2 h at a rate of 8.3 °C min^{-1}; (2) homogenization at 1025 °C for 20 h; (3) slow cooling to 500 °C at a rate of 0.1 °C min^{-1} and finally (4) cooling further to room temperature at a rate of 0.2 °C min^{-1}. Small crystals (2$-$6 mm) of CaGe$_2$ were collected and treated with an aqueous HCl solution 37% w/w (12 M) at -40°C under stirring for 7 d. The final product (GeH) was then separated

by centrifugation, washed several times with distilled water (and finally methanol), and left to dry under vacuum. No trace of a calcium signal was detected in the measured energy-dispersive x-ray spectrum of our sample, confirming the successful topotactic deintercalation of β-CaGe$_2$ and the formation of germanane (GeH) product.

The flakes were isolated via mechanical exfoliation of the synthesised powder. With an optical contrast microscope we were able to differentiate flakes with different thicknesses and we chose those with an appropriate size and shape. Ti/Au electrodes were fabricated via standard electron beam lithography using PMMA as a resist layer. Solvent residue was evaporated from the resist film by baking at 150 °C for 90 s. It was shown in [9, 16] that prolonged temperature treatment of germanane above 75°C in 5% H$_2$/Ar can cause an amorphisation process. To exclude the possibility that brief heat treatment might cause a change in the crystal structure, we made a follow-up device (sample 2) without baking, which showed quantitatively the same behaviour as sample 1 (see supplementary information). Of four prepared devices, only two were found to be electrically connected by the electrodes, presumably due to the fast oxidation of the germanane surface. Both working devices were prepared within a relatively short time period of ~12 h between the exfoliation and contact deposition in order to minimise the oxidation effect. All electrical measurements were performed in a DC current mode with the use of a Keithley 2410 source measure unit in both a vacuum chamber and a cryostat. The samples were stored and measured in vacuum with pressures of below 10^{-5} mbar in the sample space.

Acknowledgments

Author contributions

BvW, PR and DG conceived and designed the project. TG and DG synthesised the material and performed FTIR spectroscopy. GRB and GP did an XRD and DRA spectroscopy and analysis. BNM fabricated the devices. BNM and AK performed electrical characterisation, did the analysis and drafted the manuscript. CHW contributed to the analysis of optical experiments. BvW and PR contributed to the analysis, discussions and supervision of the project. All the authors gave comments on the manuscript.

References

[1] Geim A K and Grigorieva I V 2013 Van der Waals heterostructures *Nature* **499** 419–25

[2] Butler S Z *et al* 2013 Progress, challenges and opportunities in two-dimensional materials beyond graphene *ACS Nano* **7** 2898–926

[3] Li S-L, Tsukagoshi K, Orgiu E and Samori P 2016 Charge transport and mobility engineering in two-dimensional transition metal chalcogenide semiconductors *Chem. Soc. Rev.* **45** 118–51

[4] Balendhran S, Walia S, Nili H, Sriram S and Bhaskaran M 2015 Elemental analogues of graphene: silicene, germanene, stanene and phosphorene *Small* **11** 640–52

[5] Wang M, Liu L, Liu C-C and Yao Y 2016 van der waals heterostructures of germanene, stanene, and silicene with hexagonal boron nitride and their topological domain walls *Phys. Rev.* B **93** 155412

[6] Lew Yan Voon L C, Sandberg E, Aga R S and Farajian A A 2010 Hydrogen compounds of group-iv nanosheets *Appl. Phys. Lett.* **97** 163114

[7] Houssa M *et al* 2011 Electronic properties of hydrogenated silicene and germanene *Appl. Phys. Lett.* **98** 223107

[8] Shu H, Li Y, Wang S and Wang J 2015 Thickness-dependent electronic and optical properties of bernal-stacked few-layer germanane *J. Phys. Chem.* C **119** 15526–31

[9] Bianco E *et al* 2013 Stability and exfoliation of germanane: a germanium graphane analogue *ACS Nano* **7** 4414–21

[10] Qi J, Li X and Qian X 2016 Electrically controlled band gap and topological phase transition in two-dimensional multilayer germanane *Appl. Phys. Lett.* **108** 253107

[11] Amamou W *et al* 2015 Large area epitaxial germanane for electronic devices *2D Mater.* **2** 035012

[12] Zolyomi V *et al* 2014 Silicane, germanane: tight-binding and first-principles studies *2D Mater.* **1** 011005

[13] Young J R *et al* 2015 Water activated doping and transport in multilayered germanane crystals *J. Phys.: Condens. Matter* **28** 034001

[14] Sahoo N G *et al* 2016 Schottky diodes from 2d germanane *Appl. Phys. Lett.* **109** 023507

[15] Mrozel M R and Stillman G E 1996 *Properties of Gallium Arsenide* (London: INSPEC)

[16] Jiang S, Bianco E and Goldberger J E 2014 The structure and amorphization of germanane *J. Mater. Chem.* C **2** 3185–8

[17] Jiang S *et al* 2014 Improving the stability and optical properties of germanane via one-step covalent methyl-termination *Nat. Commun.* **5** 3389

[18] Liu Z *et al* 2014 GeH: a novel material as a visible-light driven photocatalyst for hydrogen evolution *Chem. Commun.* **50** 11046–8